η-η' mixing and the next-to-leading-order power correction

Tsung-Wen Yeh*
Institute of Physics, National Chiao-Tung University, Hsinchu 300, Taiwan
(Received 26 December 2001; published 7 May 2002)

The next-to-leading-order $O(1/Q^4)$ power corrections for $\eta\gamma$ and $\eta'\gamma$ form factors are evaluated and employed to explore the η-η' mixing. The parameters of the two-mixing-angle scheme are extracted from the data for form factors, two-photon decay widths, and radiative J/ψ decays. The χ^2 analysis gives the result $f_{\eta_1}=(1.16\pm0.06)f_\pi, f_{\eta_8}=(1.33\pm0.23)f_\pi, \theta_1=-9°\pm3°, \theta_8=-21.3°\pm2.3°$, where $f_{\eta_{1(8)}}$ and $\theta_{1(8)}$ are the decay constants and the mixing angles for the singlet (octet) state. In addition, we arrive at a stringent range for $f^c_{\eta'}$: -10 MeV$\leqslant f^c_{\eta'}\leqslant -4$ MeV.

DOI: 10.1103/PhysRevD.65.094019 PACS number(s): 12.38.Bx, 14.40.−n

I. INTRODUCTION

Recently, the next-to-leading-order (NLO) power correction has been shown to have an important role in understanding the exclusive processes $\gamma^*\pi\to\gamma$ [1] and $\gamma^*\pi\to\pi$ [2]. The method for calculating the NLO power correction is called the collinear expansion [1,3–6]. This power expansion method is compatible with perturbative QCD (PQCD) factorization [1,2], which gives the amplitude as a convolution of perturbatively calculable hard scattering amplitudes (the hard function) and nonperturbative hadronic wave functions (the soft function). Furthermore, it is a Feynman diagram approach such that the partonic interpretation for the NLO power correction can be preserved.

The asymptotic limit of the $\pi\gamma$ transition form factor as $2f_\pi/Q^2$ with $f_\pi=93$ MeV, is about 15% higher than the upper end of the CLEO data [7]. This deviation can be successfully explained by the NLO power correction. In addition, the NLO power correction can well describe the low energy portion of the CLEO data. Our purpose in this paper is to generalize the approach for the $\pi\gamma$ form factor to the $\eta\gamma$ and $\eta'\gamma$ form factors. The first problem we shall face is that there are many independent degrees of freedom associated with the η and η' lowest valence Fock states. The η and η' mesons are admixtures of the $SU(3)_F$ octet and singlet states; this gives eight quantities: four wave functions and four related decay constants. The η and η' mesons can also receive contributions from the $U(1)_A$ anomaly which gives intrinsic heavy quark and gluon content. To reduce the number of independent degrees of freedom, we invoke phenomenological constraints and physical assumptions about the wave functions and decay constants.

For the phenomenological constraints, we shall employ the large momentum transfer data for the $\eta\gamma$ and $\eta'\gamma$ transition form factors [7–11], the two-photon decay widths of the η and η' mesons, and the ratio $R_{J/\psi}$ of the $J/\psi\to\eta\gamma$ and $J/\psi\to\eta'\gamma$ decay widths. As for the physical assumptions we shall invoke the $SU(3)_F$ octet-singlet mixing scheme. In this mixing scheme, both η and η' are linear combinations of η_8 and η_1, the octet and singlet states in the $SU(3)_F$ representation. The mixing is controlled by the mixing angle. In the one-mixing-angle scheme, in which the octet and singlet meson states have different decay constants f_{η_8} and f_{η_1} and share a common mixing angle $\theta_8=\theta_1=\theta$, the mixing angle θ is in the range of $-20°\leqslant\theta\leqslant-10°$ [12]. In recent years, much evidence [13,14,18] has indicated that a two-mixing-angle scheme, in which the octet and singlet mixing angles θ_8 and θ_1 can take different values, is more general than the one-mixing-angle scheme. The $\eta\gamma$ and $\eta'\gamma$ form factors have been investigated by both the one-mixing-angle scheme [15–17] and two-mixing-angle scheme [14]. We would like to make a more refined analysis of these form factors by including the NLO power correction.

In this paper, we shall investigate the $\eta\gamma$ and $\eta'\gamma$ form factors and the mixing pattern of the η-η' system by employing the PQCD formula with NLO power correction in the standard hard scattering approach. We shall employ the collinear expansion to derive the NLO $[O(Q^{-4})]$ power correction for $\eta\gamma$ and $\eta'\gamma$ form factors in Sec. II. In Sec. III we shall analyze the high momentum transfer data for form factors, the two-photon decay widths, and the ratio $R_{J/\psi}$. The values of the mixing parameters are determined from a χ^2 analysis of the data. Section IV is devoted to conclusions.

II. $\eta\gamma$ AND $\eta'\gamma$ FORM FACTORS AND COLLINEAR EXPANSION

Our strategy in calculating the power corrections to the η and η' meson-photon transition form factor is to invoke the collinear expansion [1,4–6]. For simplicity, we shall first ignore the meson mass effects. That is, we choose the momentum of the initial state meson, P_1, and that of the final state photon, P_2, as

$$P_1^\mu=\left(Q,\frac{M_P^2}{2Q},0_\perp\right)\equiv p^\mu+\frac{M_P^2}{2}n^\mu\approx p^\mu,$$

$$P_2^\mu=\left(0,\frac{Q}{2},0_\perp\right)\equiv\frac{Q^2}{2}n^\mu, \tag{1}$$

such that the virtual photon has momentum $q=P_2-P_1$ with virtuality $q^2=-Q^2$ to make PQCD applicable. The vectors p and n are in the $+$ and $-$ directions in the light-cone refer-

*Electronic address: twyeh@cc.nctu.edu.tw

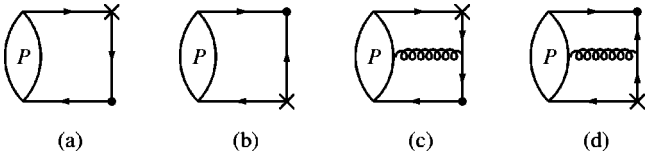

FIG. 1. The leading order diagrams for $\gamma^*\eta(\eta')\to\gamma$. The cross symbol represents the vertex of the virtual photon.

ence frame and have the properties $p^2=n^2=0$ and $p\cdot n=1$. M_P denotes the mass of the initial state meson. For the Feynman diagrams displayed in Figs. 1(a) and 1(b), the amplitudes are written as

$$A(P_1,P_2)=\int\frac{d^4k}{(2\pi)^4}\mathrm{Tr}[H(k,P_2,Q^2)\Phi(k,P_1,Q^2)] \quad (2)$$

where the trace is taken over the color and spin indices and the meson distribution amplitude (DA) $\Phi(k,P_1,Q^2)$ for the $P(=\eta,\eta')$ meson is expressed

$$\Phi(k,P_1,Q^2)=\int\frac{d^4k}{(2\pi)^4}\int d^4z e^{ik\cdot z}\langle 0|\overline{q}(0)q(z)|P\rangle. \quad (3)$$

We assign the loop momentum k for the valence antiquark and let it flow into the hard function. The hard function $H(k,P_2,Q^2)$ contains two parton-photon interaction vertices and one virtual internal parton propagator. The amplitude A contains leading, next-to-leading and higher twist contributions. The quantity twist is understood as an effective twist for nonlocal operators and is not exactly the same as the usual twist defined for local operators. The twist has different meanings for the hard and soft functions. For the hard function, the twist is defined as the power of the inverse of the photon virtuality Q, and, for the soft function, the twist represents the power of the small scale Λ with magnitude of order Λ_{QCD}. By employing collinear expansion, we can systematically separate the leading-twist (LT) contributions from the next-to-leading-twist (NLT) contributions. The LT contributions are from collinear loop momentum $\hat{k}=xp$. It is therefore convenient to parametrize the loop momentum k into

$$k^\mu=xp^\mu+\frac{k^2+k_\perp^2}{2x}n^\mu+k_\perp^\mu, \quad (4)$$

where k contains the on-shell part

$$k_L^\mu=xp^\mu+\frac{k_\perp^2}{2x}n^\mu+k_\perp^\mu \quad (5)$$

and the off-shell part

$$k_S^\mu=\frac{k^2}{2x}n^\mu. \quad (6)$$

In the first step, we expand the hard function $H(k)$ with respect to $\hat{k}$ as

$$H(k)=H(k=\hat{k})+\left.\frac{\partial H(k)}{\partial k^\alpha}\right|_{k=\hat{k}}(k-\hat{k})^\alpha+\cdots. \quad (7)$$

With the help of k_L and k_S, we can factorize the loop parton propagator $F(k)=-i/(\not{k}-i\epsilon)$ into its long distance part $F_L(k)$ and short distance part (the special propagator defined in [6]) $F_S(k)$, which are expressed as

$$F_L(k)=\frac{-i\not{k}_L}{k^2-i\epsilon},\qquad F_S(k)=\frac{-i\not{n}}{2k\cdot n-i\epsilon}. \quad (8)$$

The propagators $F_L(k)$ and $F_S(k)$ have different physical meanings. To see this, let us consider their propagation on the light cone. The integrals of $F_L(k)$ and $F_S(k)$ over $k^+=k\cdot n$ give

$$f_L(\eta,\lambda)=\int\frac{dk\cdot n}{(2\pi)}e^{ik\cdot n(\eta-\lambda)}F_L(k)\propto\theta(\eta-\lambda),$$

$$f_S(\eta,\lambda)=\int\frac{dk\cdot n}{(2\pi)}e^{ik\cdot n(\eta-\lambda)}F_S(k)\propto\delta(\eta-\lambda), \quad (9)$$

where η and λ mean the light-cone distances in the $-$ direction. It is obvious that $F_S(k)$ is not propagating on the light cone. This means that $F_S(k)$ should be included in the hard function. By dimensional counting, $F_S(k)$ is of order $O(Q^{-1})$. Therefore, including one $F_S(k)$ in the hard function causes an increase of one twist order for the hard function.

There are different effects as $F_L(k)$ and $F_S(k)$ act on the spin structures of the hard function, the terms proportional to $\not{p}$ or $\not{n}$. As $F_L(k)$ acts on $\not{p}$, its collinear part vanishes and noncollinear parts are retained:

$$F_L(k)\not{p}=-F(k)(k-\hat{k})^\alpha(i\gamma_\alpha)F_S(k)\not{p} \quad (10)$$

where the minus sign comes from the antiparticle propagator. The vertex $i\gamma_\alpha$ and short distance propagator $F_S(k)$ are then absorbed into the hard function. The factor $(k-\hat{k})^\alpha$ is included in the soft function to become a coordinate derivative of the quark fields. As $F_L(k)$ acts on $\not{n}$, its collinear part contributes to leading order. The short distance propagator $F_S(k)$ only serves to introduce the interaction term $\overline{q}\not{A}q$ for the $\not{p}$ vertex, where A^α denote the gluon fields. The total effects of $F_L(k)$ and $F_S(k)$ acting on $\not{p}$ are to include one $i\gamma_\alpha$ and one $F_S(k)$ into the hard function and to absorb the factor $(k-\hat{k})^\alpha$ and gauge fields A^α into the soft function to become a covariant derivative $D^\alpha=i\partial^\alpha-gA^\alpha$ with g the strong coupling.

The contributions from the second term of Eq. (7) and from Figs. 1(c) and 1(d) are of twist 6 or higher and will not be considered in the discussion below. The reason is that the possible nonvanishing components of γ_α in $\partial H(k)/\partial k^\alpha$ are $\alpha=+$ or $-$, but both vanish as $\partial H(k)/\partial k^\alpha$ contracts with $(k-\hat{k})^\alpha$ or $\langle 0|\overline{q}A^\alpha q|P\rangle$. We substitute the first term of Eq. (7) into the integral with the soft function and apply the identity

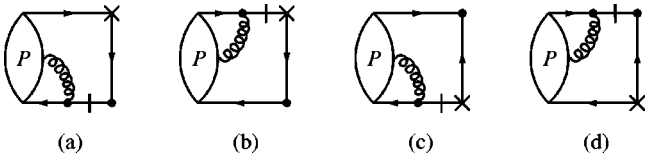

FIG. 2. The next-to-leading-twist (NLT) diagrams for $\gamma^*\eta(\eta')\to\gamma$. The propagator with one bar is the special propagator.

$$\int dx\,\delta(x-k\cdot n)=1 \tag{11}$$

to convert the loop momentum integral into the fractional variable integral. The amplitude then becomes, approximately,

$$A(P_1,P_2)\approx\int dx\mathrm{Tr}[H(x)\Phi(x)] \tag{12}$$

which contains LT and NLT contributions. The meson DA $\Phi(x)$ has the expression

$$\Phi(x)=\int_0^\infty\frac{d\lambda}{2\pi}e^{ix\lambda}\langle 0|\bar{q}(0)q(\lambda n)|P\rangle. \tag{13}$$

We now discuss how to separate the LT from the NLT contributions for amplitude A. Because the final state photon is real and has transverse polarization, the hard function $H(x)$ can have spin structures $\gamma_\perp\not{n}\gamma_\perp$, $\gamma_\perp\not{p}\not{n}$, $\gamma_\perp\not{n}\not{p}$, and $\gamma_\perp\not{p}\gamma_\perp$, where $\gamma_\perp=\gamma^\alpha$ with $\alpha=1,2$. The first spin structure leads to the LT contribution, while the second and third result in the NLT contributions. The last spin structure would lead to a next-to-next-to-leading-twist contribution and will not be considered below. To calculate the NLT contributions, we need to apply Eq. (10) to extract the contributions from the noncollinear loop momentum. As a result, we get the amplitude up to NLT as

$$A\approx\int dx\mathrm{Tr}[H(x)\Phi(x)]+\int dx\mathrm{Tr}[H_\alpha(x)w^\alpha_{\alpha'}\Phi^{\alpha'}(x)] \tag{14}$$

where the first term of the right-hand side of Eq. (14) comes from the Feynman diagrams shown in Figs. 1(a) and 1(b) and the second term from the diagrams shown in Fig. 2. The tensor $w^\alpha_{\alpha'}$ is defined as $w^\alpha_{\alpha'}=g^\alpha_{\alpha'}-p^\alpha n_{\alpha'}$. The NLT hard function $H_\alpha(x)$ is defined as

$$H_\alpha(x)=(i\gamma_\alpha)\frac{-i\not{n}}{2x}H(x)+H(x)(i\gamma_\alpha)\frac{i\not{n}}{2(1-x)} \tag{15}$$

and the NLT meson DA $\Phi^\alpha(x)$ is expressed

$$\Phi^\alpha(x)=\int_0^1dx_1\int_0^\infty\frac{d\lambda}{2\pi}\int_0^\infty\frac{d\eta}{2\pi}e^{i(x_1-x)\eta}e^{ix\lambda}\times\langle 0|\bar{q}(0)D^\alpha(\eta n)q(\lambda n)|P\rangle. \tag{16}$$

The factorization of the momentum integral is finished. To complete the factorization, we still need to perform the factorizations of the color and spin indices. To separate the color indices, we take the convention that the color factors of the hard function are extracted and absorbed into the soft function. As for the spin indices, we employ the expansion of the soft functions into their spin components

$$\Phi=\sum_\Gamma\Gamma\phi^\Gamma,$$

$$\Phi^\alpha=\sum_\Gamma\Gamma\phi^{\Gamma;\alpha}, \tag{17}$$

where Γ denotes the gamma matrix and $\phi^{\Gamma(;\alpha)}$ is the related spin component of the distribution amplitude. For a given order of $1/Q^2$, we choose the component $\phi^{\Gamma(;\alpha)}$ with lowest twist. The determination of the lowest twist $\phi^{\Gamma(;\alpha)}$ can be done as follows. First, we notice that the tensor structure of $\phi^{\Gamma(;\alpha)}$ can be expressed in terms of p, n, $d_\perp^{\alpha\beta}=g^{\alpha\beta}-p^\alpha n^\beta$, and $\epsilon_\perp^{\alpha\beta}=\epsilon^{\alpha\beta\gamma\lambda}p_\gamma n_\lambda$. The vectors p and n have dimensions $[p]=1$ and $[n]=-1$ with respect to the hard scale Q. Secondly, note that the matrix element for the soft function is written as

$$\Phi\sim\langle 0|\bar{q}q|P\rangle,$$

$$\Phi^\alpha\sim\langle 0|\bar{q}D^\alpha q|P\rangle. \tag{18}$$

From the above facts, we can derive a power counting rule as follows. Consider that $\phi^{\mu_1\cdots\mu_F;\alpha_1\cdots\alpha_B}$ has the fermion index F and the boson index B. The fermion index F arise from the spin index factorization for $2F$ fermion lines connecting the soft function and the hard function and the boson index B denotes the n_D power of momenta in the previous collinear expansion and the n_G gluon lines as $B=n_D+n_G$. We may write

$$\phi^{\mu_1\cdots\mu_F;\alpha_1\cdots\alpha_B}=\sum_i\Lambda^{\tau_i-1}e_i^{\mu_1\cdots\mu_F;\alpha_1\cdots\alpha_B}\phi^i \tag{19}$$

where Λ denotes a small scale associated with DA. The spin polarizers e_i denote the combination of vectors p^μ, n^μ, and $\gamma_\perp^\mu$. The variable τ_i represents the twist of DA ϕ^i. The restrictions over polarizers $e_i^{\mu_1\cdots\mu_F;\alpha_1\cdots\alpha_B}$ are

$$n_{\alpha_j}e_i^{\mu_1\cdots\mu_F;\alpha_1\cdots\alpha_j\cdots\alpha_B}=0, \tag{20}$$

which are due to the fact that the polarizers e_i are always projected by $w^\alpha_{\alpha'}$. The dimension of $\phi^{\mu_1\cdots\mu_F;\alpha_1\cdots\alpha_B}$ is determined by dimensional analysis,

$$d(\phi)=3F+B-1. \tag{21}$$

By equating the dimensions of both sides of Eq. (19), one can derive the minimum of τ_i,

$$\tau_i^{\min}=2F+B+\frac{1}{2}[1-(-1)^B]. \tag{22}$$

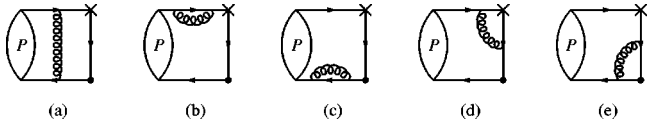

FIG. 3. The one-loop diagrams for the LT amplitude of process $\gamma^*\eta(\eta')\to\gamma$.

It is obvious from Eq. (22) that there are only finite numbers of fermion lines, gluon lines and derivatives contributing to a given power of $1/Q^2$.

We now demonstrate that the collinear expansion is compatible with the conventional approach for proving the PQCD factorization at one-loop order of the radiative correction. To show this, we consider the radiative correction for $H(x)$ as displayed in Fig. 3(a). If the radiative gluon in Fig. 3(a) is collinear with momentum $l^\alpha=(l^+,l^-,l_\perp^i)=(Q,\lambda^2/Q,\lambda)$, where $\lambda\ll Q$, the lower virtual antiquark has the momentum $(k-l)\sim(\xi Q,\lambda^2/Q,\lambda)$ with $k=xP_1$. It is obvious that the virtual antiquark in the collinear region behaves similarly to the loop antiquark in the tree amplitude. The collinear expansion for Fig. 3(a) in the collinear region is the same as the expansion for the tree diagram Fig. 1(a) in the leading configuration. To demonstrate this, we write the integrand for Fig. 3(a) as

$$I_{3a}=\int\frac{d^4l}{(2\pi)^4}\frac{g^2e^2\Gamma^{\beta\lambda}(l)}{l^2}\times\mathrm{Tr}[\gamma_\beta F(l_1)\not\epsilon F(l_3)\gamma^\mu F(l_2)\gamma_\lambda]$$
$$\equiv\int\frac{d^4l}{(2\pi)^4}\mathrm{Tr}[H_{3a}(l)\Phi_{3a}(l)], \tag{23}$$

where we have defined $l_1=k-l, l_2=(P_1-k+l)$, $l_3=P_2-k+l$,

$$H_{3a}(l)=-ie^2[\not\epsilon F(l_3)\gamma^\mu],$$
$$\Phi_{3a}(l)=\frac{ig^2\Gamma^{\beta\lambda}(l)}{l^2}[\gamma_\beta F(l_1)F(l_2)\gamma_\lambda], \tag{24}$$

and $F(l_i)=1/\not l_i$. We first expand $H_{3a}(l)$:

$$H_{3a}(l)=H_{3a}(l=\hat l)+\left.\frac{\partial H_{3a}(l)}{\partial l^\lambda}\right|_{l=\hat l}(l-\hat l)^\lambda \tag{25}$$

with $\hat l=(x-\xi)P_1$. Repeating the same considerations for the expansion of the tree amplitude, we can recast I_{3a} into

$$I_{3a}=\int d\xi[H_0^{(0)}(\xi)\Phi_{3a}(\xi)]+\int d\xi[H_\alpha^{(0)}(\xi)w^\alpha_{\alpha'}\Phi^{\alpha'}_{3a}(\xi)]+\cdots, \tag{26}$$

where

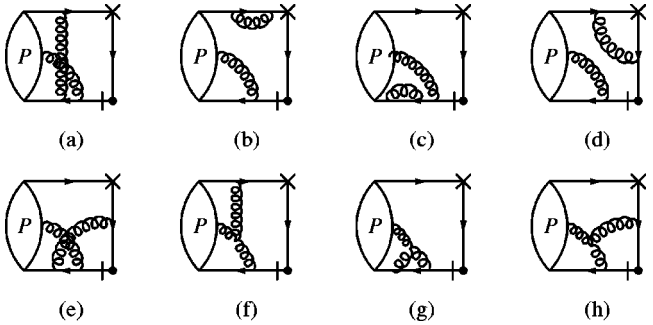

FIG. 4. The one-loop diagrams for the NLT amplitude of process $\gamma^*\eta(\eta')\to\gamma$.

$$\Phi_{3a}(\xi)=\int\frac{d\lambda}{(2\pi)}\int\frac{d^4l}{(2\pi)^4}e^{i\lambda(\xi+x-l\cdot n)}\times\left[\frac{ig^2\Gamma^{\beta\lambda}(l)}{l^2}\gamma_\beta F(l_1)F(l_2)\gamma_\lambda\right],$$
$$\Phi^{\alpha'}_{3a}(\xi)=\int\frac{d\lambda}{(2\pi)}\int\frac{d^4l}{(2\pi)^4}e^{i\lambda(\xi+x-l\cdot n)}\times\left[\frac{ig^2\Gamma^{\beta\lambda}(l)}{l^2}\gamma_\beta F(l_1)l^{\alpha'}F(l_2)\gamma_\lambda\right]. \tag{27}$$

It is obvious that both $\Phi_{3a}(\xi)$ and $\Phi^{\alpha'}_{3a}(\xi)$ are collinear divergent for collinear l. We introduce corresponding soft functions $\Phi_0^{(1)}$ and $\Phi_1^{(1)}$ to absorb $\Phi_{3a}(\xi)$ and $\Phi^{\alpha'}_{3a}(\xi)$. The corresponding tree level hard functions are denoted as $H_0^{(0)}$ and $H_1^{(0)}$, respectively. If the radiative gluons in Fig. 3(a) are soft, i.e., the gluons have momentum $l=(l^+,l^-,l_\perp)\sim(\lambda,\lambda,\lambda)$, there are no effects on power expansion. This is because the eikonal approximation up to $O(1/Q^6)$ can be applied to factorize the soft gluons from the valence quark propagator. The other two particle reducible diagrams Figs. 3(b) and 3(c) can be dealt with similarly. It is noted that the double logarithms in Figs. 3(a)–3(c) arising from the mixing contributions from the soft and collinear divergences cancel each other. In the light-cone gauge $n\cdot A=0$, Figs. 3(d) and 3(e) in the collinear region are more suppressed than Figs. 3(a)–3(c) in the collinear region by, at least, $1/Q^2$. After subtracting the soft contributions (the soft and collinear divergences) from the one-loop radiative correction diagrams Figs. 3(a)–3(c), we can obtain the one-loop corrected hard functions (LO and NLO) $H_0^{(1)}$ and $H_1^{(1)}$, separately. The analysis for the radiative corrections to $H_\alpha(x)$ is simple, since it involves only radiative corrections and has no need to consider collinear expansion. The diagrams for the radiative corrections to $H_\alpha(x)$ are shown in Fig. 4. As a result, up to first order in radiative and power corrections, we can arrive at the factorized amplitudes as

$$A^{(0)}+A^{(1)}\approx(H_0^{(0)}+H_0^{(1)})\otimes(\Phi_0^{(0)}+\Phi_0^{(1)})+(H_1^{(0)}+H_1^{(1)})\otimes(\Phi_1^{(0)}+\Phi_1^{(1)}) \tag{28}$$

where the superscript indices i $(i=0,1)$ denote the order of radiative correction and the subscript indices j $(j=0,1)$ mean the order of power correction. The notation $\otimes$ represents the convolution integral and the trace over the color and spin indices. To prove PQCD factorization, we need to generalize the one-loop factorization to arbitrary orders. It can be done straightforwardly [19–22].

For convenience, we may write the amplitude as

$$A(\gamma^*P\to\gamma)=-ie^2\epsilon_{\mu\alpha\beta\lambda}P_1^\alpha P_2^\beta\epsilon^\lambda F_{P\gamma}(Q^2), \tag{29}$$

where ϵ^λ denotes the polarization vector of the final state photon. The form factors are expressed in terms of the octet and singlet components:

$$F_{P\gamma}(Q^2)=\sum_{i=8,1} a_P^{P_i}F_{P_i\gamma}(Q^2), \tag{30}$$

where the expansion coefficients $a_P^{P_i}, P=\eta,\eta', i=8,1$, depend on the mixing scheme (see the next section). Because of the η-η' mixing, we take the octet and singlet states as the basis for our investigation of the form factors. The superscript $i=8$ or 1 denotes the contributions from octet or singlet current (see notation below). The leading order of $F_{P_i\gamma}(Q^2)$ is calculated from Figs. 1(a) and 1(b) and takes the expression

$$F_{P_i\gamma}^{\rm LO}(Q^2)=4C_i\int_0^1 dx\frac{\phi_{P_i}(x)}{Q^2x(1-x)}, \tag{31}$$

where the charge factors are defined as $C_8=(e_u^2+e_d^2-2e_s^2)/\sqrt{6}$ and $C_1=(e_u^2+e_d^2+e_s^2)/\sqrt{3}$. The NLO of $F_{P_i\gamma}(Q^2)$ is evaluated from Fig. 2 as

$$F_{P_i\gamma}^{\rm NLO}(Q^2)=-16C_i\int_0^1 dx\frac{[G_{P_i}(x)+\tilde{G}_{P_i}(x)(1-2x)]}{Q^4x(1-x)}. \tag{32}$$

We have taken the symmetry between the exchange of $x\leftrightarrow(1-x)$ for $\phi_{P_i}(x)$, $G_{P_i}(x)$, and $\tilde{G}_{P_i}(x)$. The relevant DAs are expressed explicitly as follows:

$$\phi_{P_i}(x)=-i\frac{1}{4}\int_0^\infty\frac{d\lambda}{(2\pi)}e^{i\lambda x}\langle 0|J_5^i(0,\lambda n)|P_i(P_1)\rangle, \tag{33}$$

$$G_{P_i}(x)=-\frac{1}{8}\epsilon_\perp^{\alpha\beta}\int_0^1 dx_1\int_0^\infty\frac{d\lambda}{(2\pi)}\frac{d\eta}{(2\pi)}e^{i\eta(x_1-x)}\times e^{i\lambda x}\langle 0|J_{\alpha\beta}^i(0,\eta n,\lambda n)|P_i(P_1)\rangle, \tag{34}$$

$$\tilde{G}_P^i(x)=-\frac{i}{8}d_\perp^{\alpha\beta}\int_0^1 dx_1\int_0^\infty\frac{d\lambda}{(2\pi)}\frac{d\eta}{(2\pi)}e^{i\eta(x_1-x)}\times e^{i\lambda x}\langle 0|J_{\alpha\beta5}^i(0,\eta n,\lambda n)|P_i(P_1)\rangle, \tag{35}$$

where nonlocal currents are defined as

$$J_5^8(0,\lambda n)=\frac{1}{\sqrt{6}}[\bar{u}(0)\gamma_5\not{n}u(\lambda n)+\bar{d}(0)\gamma_5\not{n}d(\lambda n)-2\bar{s}(0)\gamma_5\not{n}s(\lambda n)],$$

$$J_5^1(0,\lambda n)=\frac{1}{\sqrt{3}}[\bar{u}(0)\gamma_5\not{n}u(\lambda n)+\bar{d}(0)\gamma_5\not{n}d(\lambda n)+\bar{s}(0)\gamma_5\not{n}s(\lambda n)],$$

$$J_{\alpha\beta}^8(0,\eta n,\lambda n)=\frac{1}{\sqrt{6}}[\bar{u}(0)\gamma_\alpha D_\beta(\eta n)u(\lambda n)+\bar{d}(0)\gamma_\alpha D_\beta(\eta n)d(\lambda n)-2\bar{s}(0)\gamma_\alpha D_\beta(\eta n)s(\lambda n)],$$

$$J_{\alpha\beta}^1(0,\eta n,\lambda n)=\frac{1}{\sqrt{3}}[\bar{u}(0)\gamma_\alpha D_\beta(\eta n)u(\lambda n)+\bar{d}(0)\gamma_\alpha D_\beta(\eta n)d(\lambda n)+\bar{s}(0)\gamma_\alpha D_\beta(\eta n)s(\lambda n)],$$

$$J_{\alpha\beta5}^8(0,\eta n,\lambda n)=\frac{1}{\sqrt{6}}[\bar{u}(0)\gamma_5\gamma_\alpha D_\beta(\eta n)u(\lambda n)+\bar{d}(0)\gamma_5\gamma_\alpha D_\beta(\eta n)d(\lambda n)-2\bar{s}(0)\gamma_5\gamma_\alpha D_\beta(\eta n)s(\lambda n)],$$

$$J_{\alpha\beta5}^1(0,\eta n,\lambda n)=\frac{1}{\sqrt{3}}[\bar{u}(0)\gamma_5\gamma_\alpha D_\beta(\eta n)u(\lambda n)+\bar{d}(0)\gamma_5\gamma_\alpha D_\beta(\eta n)d(\lambda n)+\bar{s}(0)\gamma_5\gamma_\alpha D_\beta(\eta n)s(\lambda n)]. \tag{36}$$

Because of the factor $1-2x$ for $\tilde{G}_{P_i}$, G_{P_i} become dominant. The normalizations of ϕ_P^i and G_P^i are determined from the leptonic weak decay and the axial anomaly for P_i meson, respectively. This is similar to the pion case [1].

III. THE MIXING SCHEMES

We employ the $SU(3)_F$ octet and singlet states to describe the η-η' system. The η and η' meson states can be described by means of the octet and singlet states $|\eta_8\rangle$ and $|\eta_1\rangle$ through the one-mixing-angle scheme:

$$|\eta\rangle=\cos\theta|\eta_8\rangle-\sin\theta|\eta_1\rangle,$$
$$|\eta'\rangle=\sin\theta|\eta_8\rangle+\cos\theta|\eta_1\rangle, \tag{37}$$

where the mixing angle θ controls the relative strength. With the mixing, the $\eta\gamma$ and $\eta'\gamma$ form factors take the expressions

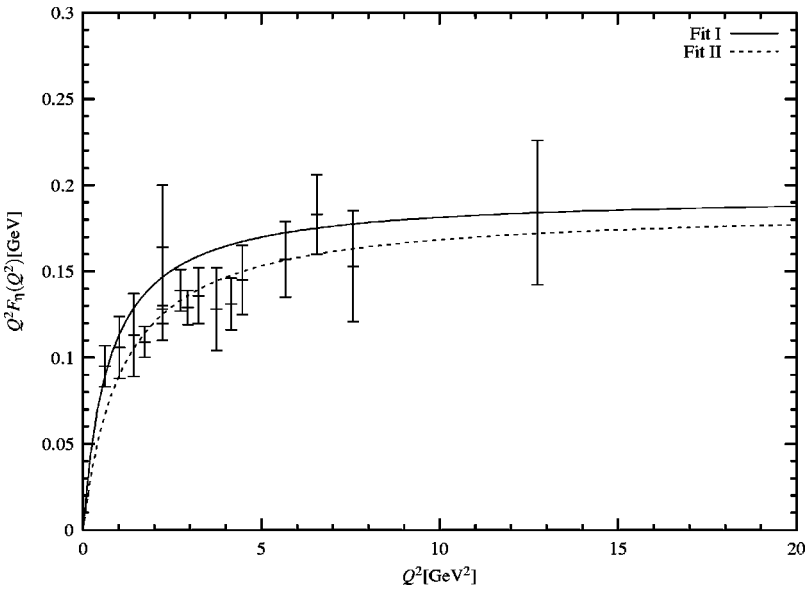

FIG. 5. The results of the χ^2 fit to the $\eta\gamma$ transition form factor within the one-mixing-angle scheme (the solid line) and the two-mixing-angle scheme (the dashed line). The data points are taken from [7–11].

$$F_{\eta\gamma}(Q^2)=\cos\theta F_{\eta_8\gamma}(Q^2)-\sin\theta F_{\eta_1\gamma}(Q^2),$$

$$F_{\eta'\gamma}(Q^2)=\sin\theta F_{\eta_8\gamma}(Q^2)+\cos\theta F_{\eta_1\gamma}(Q^2). \tag{38}$$

To proceed, we also assume that the octet and singlet DAs take asymptotic form. Therefore, we have $\phi_{\eta_i}(x)=3f_{\eta_i}x(1-x)/\sqrt{2}$ and $G_{\eta_i}(x)=3\sqrt{2}\pi^2 f_{\eta_i}^3 x(1-x)$. The form factors $F_{\eta_i\gamma}(Q^2)$ $(i=8,1)$ are simplified by substituting $\phi_{\eta_i}(x)$ and $G_{\eta_i}(x)$:

$$F_{\eta_i\gamma}(Q^2)=4C_i\int dx\frac{1}{x(1-x)}\left[\frac{\phi_{\eta_i}(x)}{Q^2}-4\frac{G_{\eta_i}(x)}{Q^4}\right]$$

$$=6\sqrt{2}C_i\frac{f_{\eta_i}}{Q^2}\left[1-\frac{8\pi^2 f_{\eta_i}^2}{Q^2}\right]. \tag{39}$$

Using Eq. (39) in Eq. (38), we can derive the coefficients $a_P^{P_i}$ in Eq. (30).

To compare the form factors with the data, we extrapolate the form factors to all orders:

$$F_{\eta_i\gamma}(Q^2)=\frac{6\sqrt{2}C_i f_{\eta_i}}{Q^2+8\pi^2 f_{\eta_i}^2}. \tag{40}$$

This formula gives theoretical support to the approach using the interpolating formula for the $\eta\gamma$ and $\eta'\gamma$ form factors [18].

The decay constants $f_{\eta_i}, i=8,1$, and the mixing angle θ will be determined by a least χ^2 fit to the transition form factor data above 1 GeV^2 and the two-photon decay widths [23]

$$\Gamma[\eta\to\gamma\gamma]=0.46\pm0.04 \text{ keV},$$

$$\Gamma[\eta'\to\gamma\gamma]=4.28\pm0.19 \text{ keV}. \tag{41}$$

The decay rates have the theoretical expressions

$$\Gamma[\eta\to\gamma\gamma]=\frac{9\alpha^2}{32\pi^3}M_\eta^3\left[\frac{C_8 f_{\eta'}^1-C_1 f_{\eta'}^8}{f_{\eta'}^1 f_\eta^8-f_{\eta'}^8 f_\eta^1}\right]^2,$$

$$\Gamma[\eta'\to\gamma\gamma]=\frac{9\alpha^2}{32\pi^3}M_{\eta'}^3\left[\frac{-C_8 f_\eta^1+C_1 f_\eta^8}{f_{\eta'}^1 f_\eta^8-f_{\eta'}^8 f_\eta^1}\right]^2, \tag{42}$$

where the decay constants are defined as

$$f_\eta^8=f_{\eta_1}\cos\theta, \quad f_\eta^1=-f_{\eta_1}\sin\theta,$$

$$f_{\eta'}^8=f_{\eta_1}\sin\theta, \quad f_{\eta'}^1=f_{\eta_1}\cos\theta. \tag{43}$$

The χ^2 fit results are shown as fit I in Figs. 5 and 6 and in Table I. It is seen that fit I is in good agreement with the data for the form factors. To test the fit parameters, we employ the ratio of the decay rates for J/ψ in $\eta'\gamma$ and $\eta\gamma$:

$$R_{J/\psi}=\frac{\Gamma(J/\psi\to\eta'\gamma)}{\Gamma(J/\psi\to\eta\gamma)}=5.0\pm0.6. \tag{44}$$

It is usually assumed that the radiative $J/\psi\to\eta(\eta')\gamma$ decays are dominated by nonperturbative gluon matrix elements $\langle 0|G\tilde{G}|\eta'\rangle$ and $\langle 0|G\tilde{G}|\eta\rangle$ such that the ratio takes the expression [24]

$$R_{J/\psi}=\left(\frac{M_{\eta'}^2(f_{\eta'}^8+\sqrt{2}f_{\eta'}^1)}{M_\eta^2(f_\eta^8+\sqrt{2}f_\eta^1)}\right)^2\left(\frac{p_{\eta'}}{p_\eta}\right)^3 \tag{45}$$

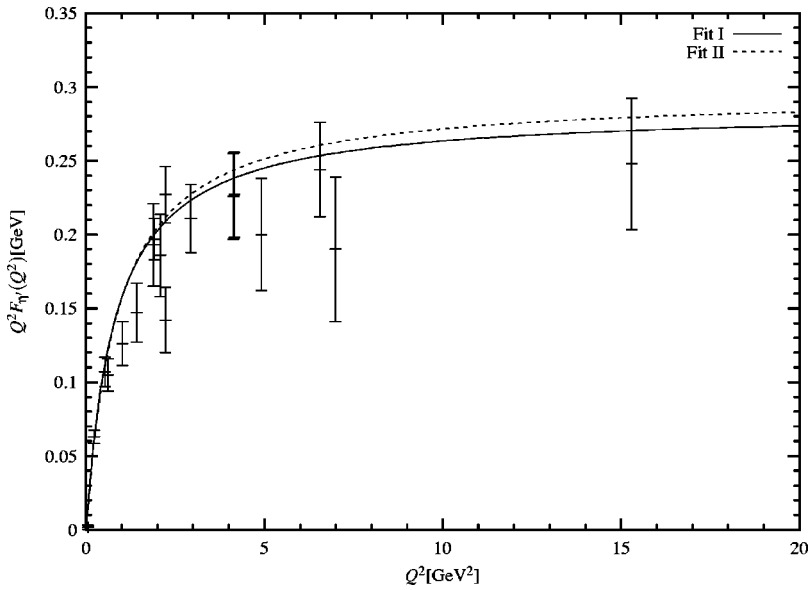

FIG. 6. The results of the χ^2 fit to the $\eta'\gamma$ transition form factor within the one-mixing-angle scheme (the solid line) and the two-mixing-angle scheme (the dashed line). The data points are taken from [7–11].

with $p_P = M_{J/\psi}(1-M_P^2/M_{J/\psi}^2)/2$ being the three-momentum of the P meson. Our fit result is close to the one obtained from chiral perturbation theory (χPT), except for the octet decay constant $f_{\eta_8} = f_\pi < 1.28 f_\pi$,

$$\chi PT: \theta \approx -20^\circ \quad \text{to} \quad -10^\circ,$$

$$f_{\eta_8} = 1.28 f_\pi, \quad f_{\eta_1} \approx 1.1 f_\pi. \tag{46}$$

The octet decay constant f_{η_8} is calculable by χPT up to the one-loop approximation

$$f_{\eta_8} \approx \left[1 - \frac{M_K^2}{(4\pi f_\pi)^2} \ln \frac{M_K^2}{(4\pi f_\pi)^2} + \frac{M_\pi^2}{(4\pi f_\pi)^2}\right] \times f_\pi = 1.28 f_\pi. \tag{47}$$

It is noted that the predicted results for $\Gamma(\eta \to \gamma\gamma)$, $\Gamma(\eta' \to \gamma\gamma)$, and $R_{J/\psi}$ shown in Table I are close to the experimental values within 1σ accuracy.

Recently, it has been proposed [13,14,18] that $|\eta\rangle$ and $|\eta'\rangle$ can mix through a two mixing-angle-scheme as

$$|\eta\rangle = \cos\theta_8 |\eta_8\rangle - \sin\theta_1 |\eta_1\rangle,$$

$$|\eta'\rangle = \sin\theta_8 |\eta_8\rangle + \cos\theta_1 |\eta_1\rangle, \tag{48}$$

where θ_i denote the mixing angles. Using this mixing scheme, the $\eta\gamma$ and $\eta'\gamma$ form factors can be expressed, respectively, as

$$F_{\eta\gamma}(Q^2) = \cos\theta_8 F_{\eta_8\gamma}(Q^2) - \sin\theta_1 F_{\eta_1\gamma}(Q^2),$$

$$F_{\eta'\gamma}(Q^2) = \sin\theta_8 F_{\eta_8\gamma}(Q^2) + \cos\theta_1 F_{\eta_1\gamma}(Q^2). \tag{49}$$

The form factors $F_{\eta_i\gamma}(Q^2)$ are the same as those in the one-mixing-angle scheme. We first change the values of f_{η_i} and θ_i to fit the data. The χ^2 fit result is shown as fit II in Figs. 5 and 6 and Table I. From fit I and fit II in Table I, it is found that the two-mixing-angle scheme is better in accuracy than the one-mixing-angle scheme by 100%. This is close to the investigations of [13,14,18].

A large value of $f_{\eta'}^c = \cos\theta_1 f_{\eta_c}$ [25,26], which is responsible for the intrinsic charm content of the η' meson, has been proposed to resolve the large branching ratios $\mathrm{BR}(B \to \eta' K)$ and $\mathrm{BR}(B \to X_s\gamma)$. We may explore this within our approach by adding intrinsic charm content into our formalism. The effects of the intrinsic charm content are similar to that of the singlet component. That means one can replace f_{η_1} with $f_{\eta_c} = f_{\eta'}^c/\cos\theta_1$, the decay constant for intrinsic charm for the corresponding singlet terms. That is the part of the form factors from the intrinsic charm, with the expression

TABLE I. The results of the χ^2 fit to the $\eta\gamma$ and $\eta'\gamma$ transition form factors and the two-photon widths within the one- and two-mixing-angle schemes.

	f_{η_8}/f_π	f_{η_1}/f_π	θ_8	θ_1	$\Gamma(\eta\to 2\gamma)$ (keV)	$\Gamma(\eta'\to 2\gamma)$ (keV)	$R_{J/\psi}$	χ^2 per degree of freedom
Fit I	0.99	1.08	-16.4°	-16.4°	0.49	4.47	5.6	64/31
Fit II	1.32	1.16	-22.3°	-9.1°	0.50	4.34	4.4	32/31

TABLE II. The results of the χ^2 fit to the $\eta\gamma$ and $\eta'\gamma$ transition form factors within the one- and two-mixing-angle schemes with or without intrinsic charm content.

	f_{η_8}/f_π	f_{η_1}/f_π	f_{η_c}(MeV)	θ_8	θ_1	χ^2 per degree of freedom
Fit I	0.99	1.08	0	$-16.4°$	$-16.4°$	61/29
Fit I	0.99	1.08	-8	$-16.4°$	$-16.4°$	34/29
Fit II	1.32	1.16	0	$-22.3°$	$-9.1°$	31/29
Fit II	1.32	1.16	-5.6	$-22.3°$	$-9.1°$	19/29

$$F_{\eta_c\gamma}(Q^2)=4e_c^2\int\frac{dx}{x(1-x)}\left[\frac{\phi_{\eta_c}(x)}{Q^2}-4\frac{G_{\eta_c}(x)}{Q^4}\right] \quad (50)$$

where $e_c=2/3$ and the related DAs are $\phi_{\eta_c}(x)=3f_{\eta_c}x(1-x)/\sqrt{2}$ and $G_{\eta_c}(x)=3\sqrt{2}\pi^2 f_{\eta_c}^2 x(1-x)$. The effect from the large value of the charm quark mass has been absorbed into the twist-4 DA $G_{\eta_c}(x)$ [1]. After including the contribution of the intrinsic charm, the $\eta\gamma$ and $\eta'\gamma$ form factors then become

$$\begin{aligned}F_{\eta\gamma}(Q^2)&=\cos\theta_8 F_{\eta_8\gamma}(Q^2)\\&\quad-\sin\theta_1[F_{\eta_1\gamma}(Q^2)+F_{\eta_c\gamma}(Q^2)],\\F_{\eta'\gamma}(Q^2)&=\sin\theta_8 F_{\eta_8\gamma}(Q^2)\\&\quad+\cos\theta_1[F_{\eta_1\gamma}(Q^2)+F_{\eta_c\gamma}(Q^2)].\end{aligned} \quad (51)$$

As in the case of the octet and singlet form factors, the extrapolation of $F_{\eta_c\gamma}(Q^2)$ to all orders is implied. It is clear from Eq. (51) that the form factor $F_{\eta'\gamma}(Q^2)$ has a larger dependence on f_{η_c} than $F_{\eta\gamma}(Q^2)$. We make a least χ^2 fit to the form factor data to determine possible values of f_{η_c} by keeping the other parameters fixed. From Table II, one may see that including the intrinsic charm content can indeed improve the accuracy. This shows that our formalism is consistent with perturbation theory and that the higher Fock state can be reasonably added in. As shown below, the allowed value for f_{η_c} is less than f_π. In literature [14,18,25,26], f_{η_c} is proposed in the range $-140\ \text{MeV}\leqslant f_{\eta_c}\leqslant 15\ \text{MeV}$. To test this, we plot in Fig. 7 the χ^2 distribution for each set of mixing parameters listed in Table II over a wide range of $-140\ \text{MeV}\leqslant f_{\eta_c}\leqslant 140\ \text{MeV}$. It is seen that the range of $f_{\eta_c}-10\ \text{MeV}\leqslant f_{\eta_c}\leqslant -4\ \text{MeV}$ is allowed by the data. Because the value of $\cos\theta_1$ is close to unity, $f^c_{\eta'}$ is almost equal to f_{η_c}.

From the above analysis, one may see that combining the high energy data and the low energy experiment can result in constraints on the mixing parameters in a very efficient way. We can give a general analysis for the two-mixing-angle scheme. We shall investigate the χ^2 distributions of the mixing parameters. The procedure of analysis is as follows. We first separate the data into two groups. The data for the form factors, the two-photon decay rates, and the ratio for J/ψ radiative decays are denoted as set I while the latter two data are chosen as set II. We then determine the least χ^2 values for sets I and II. The reason for separating the data into set I and set II is that neither set I nor set II can completely constrain the parameters. The parameters located within 1σ accuracy of set I still have large uncertainties and require further restrictions, which can be obtained from the data set II.

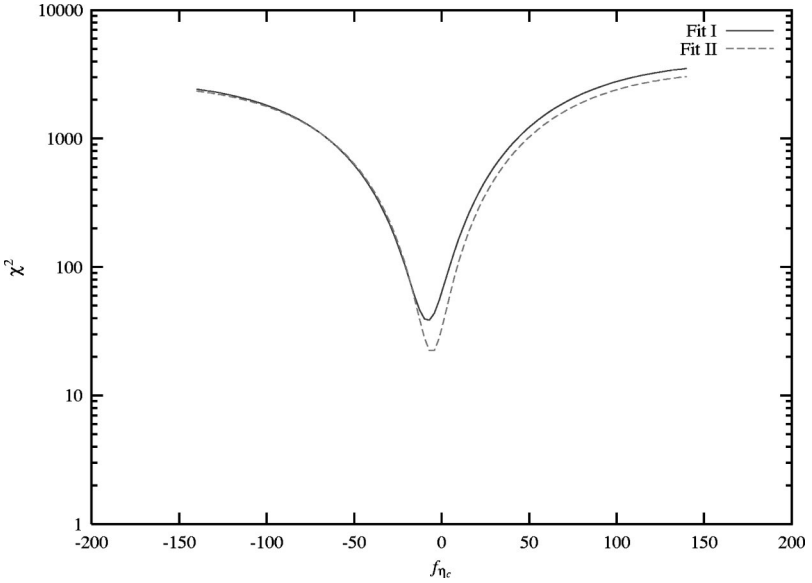

FIG. 7. The plot of the χ^2 distribution vs f_{η_c}. The χ^2 values are evaluated for the data for form factors obtained by employing the sets of parameters listed in Table I.

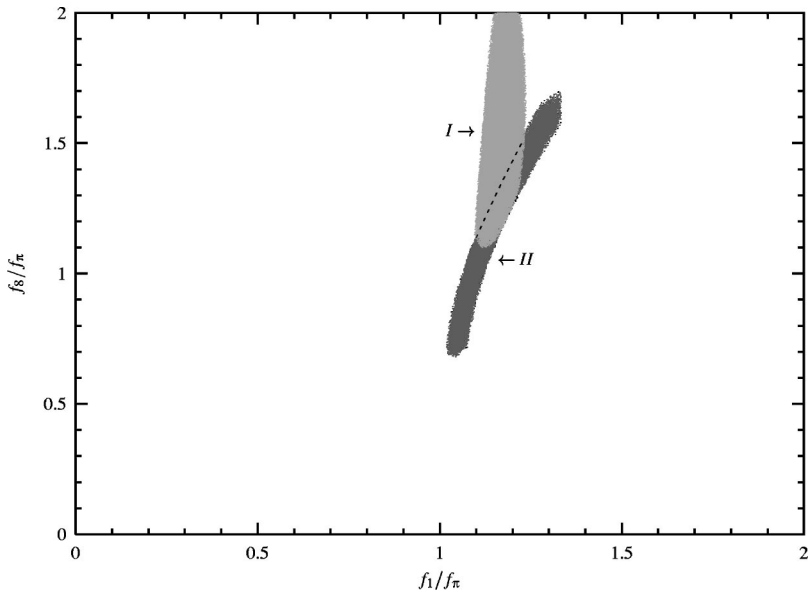

FIG. 8. The plot of f_{η_1} versus f_{η_8} from the χ^2 analysis for the data sets I and II. The regions denoted as I and II represent the allowable values for f_{η_1} and f_{η_8} within 1σ error for corresponding data sets I and II.

To be more explicit, we plot the allowable regions for the mixing parameters within 1σ error with respect to those values associated with the minimal χ^2 points. As shown in Figs. 8 and 9, both allowable regions for data sets I and II are large while their intersections are rather restricted. The reason for this fact is easily understood. Within the data set I, the experimental errors are shared for high and low energy data. Because the χ^2 distribution can only measure the correlations between the mixing parameters, the aim of constraining each parameter in an independent way cannot be met, and only partial restrictions over the correlations of the parameters can be derived. This can be seen from Fig. 8, in which the f_8 parameter is not contrained in a reasonable way. To compensate this flaw, we note that the χ^2 distribution of data set II can intersect with the χ^2 distribution of data set I. The intersections between the two χ^2 distributions can give better constraints on the parameters than the data set I or II. One should note that, although the data set II is a subset of the data set I, χ^2 distribution of the data set II is not necessarily a subset of the χ^2 distribution of data set I, since the effects of correlations between the parameters are different for the two data sets. From the overlapping regions of the data sets I and II at 1σ error, we may extract from Figs. 8 and 9 the allowable regions for the mixing parameters. In Fig. 8, we plot the possible allowable ranges for f_{η_8} and f_{η_1}. It can be observed from Fig. 8 that the overlapping region for f_{η_8} and f_{η_1} is quite stringent: $1.1 \leqslant f_{\eta_8}/f_\pi \leqslant 1.56$ and $1.1 \leqslant f_{\eta_1}/f_\pi \leqslant 1.22$. Figure 9 shows the allowable region for θ_1 and θ_8 from both data set I and set II. The overlapping region indicates that $-12° \leqslant \theta_1 \leqslant -6°$ and $-23.6° \leqslant \theta_8 \leqslant -19°$.

Combining Figs. 8 and 9, we may derive the $Q^2 \to \infty$ limits of the scaled $\eta\gamma$ and $\eta'\gamma$ form factors:

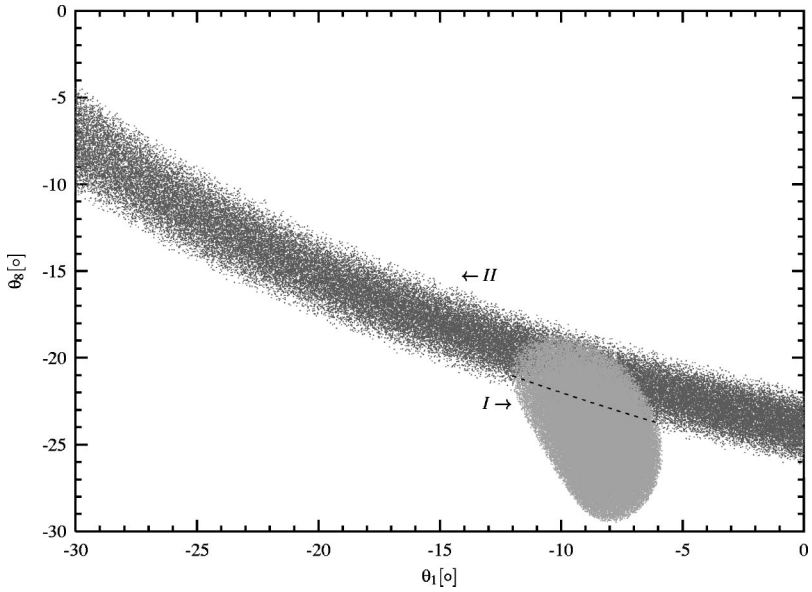

FIG. 9. The plot of θ_1 versus θ_8 from the χ^2 analysis for the data sets I and II. The regions denoted as I and II represent the allowable values for θ_1 and θ_8 within 1σ error for the corresponding data sets I and II.

$$Q^2 F_{\eta\gamma}(Q^2)|_{Q^2\to\infty} = \frac{2}{\sqrt{3}}[f_{\eta_8}\cos\theta_8 - 2\sqrt{2} f_{\eta_1}\sin\theta_1]$$
$$= 189 \pm 46 \ \text{MeV},$$
$$Q^2 F_{\eta'\gamma}(Q^2)|_{Q^2\to\infty} = \frac{2}{\sqrt{3}}[f_{\eta_8}\sin\theta_8 + 2\sqrt{2} f_{\eta_1}\cos\theta_1]$$
$$= 295 \pm 35 \ \text{MeV}. \quad (52)$$

The error in the scaled $\eta\gamma$ form factor being larger than that of the scaled $\eta'\gamma$ form factor is because the errors in the data for the $\eta\gamma$ and $\eta'\gamma$ form factors are shared in our analysis. This is consistent with the concept of η-η' mixing.

IV. CONCLUSIONS

We have shown that the collinear expansion for $\gamma^*\eta(\eta')\to\gamma$ can be systematically performed in compatibility with PQCD factorization. The $O(Q^{-4})$ power corrections for $F_{\eta\gamma}(Q^2)$ and $F_{\eta'\gamma}(Q^2)$ were evaluated. The magnitudes of NLO power corrections were determined.

We made a general analysis for the allowed values for the mixing parameters by combining the high and low energy data. Except for f_{η_8}, the other three parameters $f_{\eta_1}, \theta_{8(1)}$ can be constrained in a reasonable region. The large error for the fit of f_{η_8} is mainly from the experimental error and can be improved by future experiments with higher accuracy. At present, we would invoke the chiral perturbation theory calculation for f_{η_8}.

We have also shown that the intrinsic charm content of η' meson has little contribution. Any sizable contribution from the intrinsic charm would lead to a large χ^2 value as shown in Fig. 7. Of course, further investigations are required on this point, if more accurate form factor data become available.

So far, we have not considered the finite meson mass effects for the $\eta\gamma$ and $\eta'\gamma$ form factors. At first glance, the meson mass effects cannot be safely ignored. Because the values of η and η' meson masses are as large as $M_\eta = 547$ MeV and $M_{\eta'} = 958$ MeV, power corrections from the mass effects of order $O(M_P^2/Q^2)$ and $O(M_P^2\Lambda^2/Q^4)$ are also important. The corrections $O(M_P^2/Q^2)$ are of kinematic type. This is similar to Nachtmann's correction for deep inelastic scattering [27] and can be negligible. The second type of correction $O(M_P^2\Lambda^2/Q^4)$ is dynamic and it can be argued that they are of twist 6 at least. This is because the associated spin projector is $\not{n}\gamma_5$ (cf. the leading spin projector $\not{p}\gamma_5$), which will introduce two additional F_S propagators into the related hard function. As a result, the dynamical type meson mass corrections are of order $O(M_P^2\Lambda^4/Q^6)$. Of course, a complete analysis for these meson mass effects is important.

ACKNOWLEDGMENTS

This work was supported in part by the National Science Council of R.O.C. under Grant No. NSC89-2811-M-009-0024.

[1] T.W. Yeh, hep-ph/0105171.
[2] T.W. Yeh, Phys. Rev. D **65**, 074016 (2002).
[3] T.W. Yeh, contribution to the Proceedings of the Fourth International Workshop on *B* Physics and *CP* Violation, Ise-Shima, Japan, 2001.
[4] R.K. Ellis, W. Furmanski, and R. Petronzio, Nucl. Phys. **B207**, 1 (1982).
[5] R.K. Ellis, W. Furmanski, and R. Petronzio, Nucl. Phys. **B212**, 29 (1983).
[6] J. Qiu, Phys. Rev. D **42**, 30 (1990).
[7] CLEO Collaboration, J. Gronberg *et al.*, Phys. Rev. D **57**, 33 (1998).
[8] L3 Collaboration, M. Acciarri *et al.*, Phys. Lett. B **418**, 399 (1998).
[9] CELLO Collaboration, H.J. Behrend *et al.*, Z. Phys. C **49**, 401 (1991).
[10] TPC/Two Gamma Collaboration, H. Aihara *et al.*, Phys. Rev. Lett. **64**, 172 (1990).
[11] PLUTO Collaboration, C. Berger *et al.*, Phys. Lett. **142B**, 125 (1984).
[12] F.J. Gilman and R. Kauffman, Phys. Rev. D **36**, 2761 (1987); **37**, 3348(E) (1988).
[13] H. Leutwyler, Nucl. Phys. B (Proc. Suppl.) **64**, 223 (1998).
[14] T. Feldmann and P. Kroll, Eur. Phys. J. C **5**, 327 (1998).
[15] R. Jakob, P. Kroll, and M. Raulfs, J. Phys. G **22**, 45 (1996).
[16] V.V. Anisovich, D.I. Melikhov, and V.A. Nikonov, Phys. Rev. D **55**, 2918 (1997).
[17] L. Ametller, J. Bijinens, A. Bramon, and F. Cornet, Phys. Rev. D **45**, 986 (1992).
[18] T. Feldmann and P. Kroll, Phys. Rev. D **58**, 057501 (1998).
[19] P. Ball, J.M. Frere, and M. Tytgat, Phys. Lett. B **365**, 367 (1996).
[20] J. Botts and G. Sterman, Nucl. Phys. **B325**, 62 (1989).
[21] H. Li and G. Sterman, Nucl. Phys. **B381**, 129 (1992).
[22] T.W. Yeh (in preparation).
[23] Particle Data Group, J. Bartels *et al.*, Eur. Phys. J. C **15**, 1 (2000).
[24] A.V. Kiselev and V.A. Petrov, Z. Phys. C **58**, 595 (1993).
[25] I. Halperin and A. Zhitnitsky, Phys. Rev. D **56**, 7247 (1997).
[26] H. Cheng and B. Tseng, Phys. Lett. B **415**, 263 (1997).
[27] O. Nachtmann, Nucl. Phys. **B63**, 237 (1973).